Electrogeneration of a free-standing cytochrome *c* – silica matrix at a soft electrified interface

Alonso Gamero-Quijano,[1] Manuel Dossot,[2] Alain Walcarius,[2] Micheál D. Scanlon,[1]*
Grégoire Herzog[2]*

[1] The Bernal Institute and Department of Chemical Sciences, School of Natural Sciences, University of Limerick (UL), Limerick V94 T9PX, Ireland

[2] Université de Lorraine, CNRS, LCPME, F-54000 Nancy, France

*Corresponding authors: micheal.scanlon@ul.ie; gregoire.herzog@univ-lorraine.fr

Abstract

Interactions of a protein with a solid-liquid or a liquid-liquid interface may destabilise its conformation and hence result in a loss of biological activity. We propose here a method for the immobilisaiton of protein at an electrified liquid-liquid interface while maintaining it's native conformation. Cytochrome *c* (Cyt *c*) is encapsulated in a silica matrix through an electrochemical process at an electrified liquid-liquid interface. Silica condensation is triggered by the interfacial transfer of cationic surfactant, cetyltrimethylammonium, at the lower end of the interfacial potential window. Cyt *c* is then adsorbed on the previously electrodeposited silica layer, when the interfacial potential, $\Delta_o^w\phi$, is at the positive end of the potential window. By cycling the potential window back and forth, silica electrodeposition and Cyt *c* adsorption occurs sequentially as demonstrated by *in situ* UV-vis absorbance spectroscopy. After collection from the liquid-liquid interface, the Cyt *c* – silica matrix is characterised *ex situ* by UV-vis diffuse reflectance spectroscopy, confocal Raman microscopy and fluorescence microscopy, showing that the protein maintained its tertiary structure during the encapsulation process. The absence of denaturation is further confirmed *in situ* by the absence of electrocatalytic activity towards O_2, signalling Cyt *c* denaturation. This method of protein encapsulation may be used for other proteins in the development of biphasic bioelectrosynthesis or bioelectrocatalysis applications.

Introduction

Immobilisation of proteins is often sought for applications in the fields of bioanalysis and biocatalysis.[1] Proteins immobilised onto a substrate offers a more convenient handling, provides a separation from the product and improves the storage and operational stability over time.[2] Nevertheless, the control of the protein environment during and after the immobilisation process ensures that the immobilised protein will retain its biological activity. Indeed, hydrophobic and electrostatic interactions of a protein at a solid-liquid or liquid-liquid interface may impact the stability of its secondary structure and hence lead to a loss of biological activity.[3] Furthermore, the direct environment of the protein (*e.g.* pH, ionic strength, temperature, solvent polarity, protein isoelectric point, size, and shape…) can alter the adsorption. In the field of bioelectrocatalysis, various strategies have been envisaged to create a favourable environment to maintain the protein conformation and hence activity.[4]

The behaviour of various proteins at polarised liquid-liquid interfaces (a.k.a. interfaces between two immiscible electrolyte solutions, ITIES) has been investigated by electrochemical means.[5,6] It was shown that proteins such as cytochrome *c*,[7–9] insulin,[10] haemoglobin,[11,12] lysozyme,[13] myoglobin,[14] albumin,[15] ferritin,[16] and thrombin,[17] behaved in a similar manner at the ITIES. Adsorption of the protein at the ITIES was induced by the application of a potential difference greater than the potential of zero charge (PZC). At the positive end of the potential window, the transfer of the anion of the background electrolyte of the organic phase was assisted by the adsorbed protein solution through hydrophobic and electrostatic interactions with the partially unfolded proteins as demonstrated experimentally[18–20] and supported by molecular dynamics simulations.[21,22] In the case of cytochrome *c*, partial denaturation of the protein was responsible for a bioelectrocatalytic O_2 reduction reaction observed at the ITIES.[23] Preventing protein denaturation at the ITIES remains a challenge. Protein encapsulation within biocompatible silica matrices may solve this issue.[24–26] For instance, Montilla *et al.* have shown that Cyt *c* species present long-term stability if they are encapsulated inside silica matrices, made of a mixture of silanes and methylated silanes.[27,28] Recently, Poltorak *et al.* reported the encapsulation of three proteins (haemoglobin, acid phosphatase and α-amylase) in a silica matrix by a co-deposition process at the ITIES under acidic conditions.[29,30] After encapsulation, these proteins presented interfacial activity towards ion-transfer reactions. Thus, the encapsulation within silica networks might provide soft immobilisation conditions at the ITIES delaying the denaturation process during the external biasing at positive potentials.

Furthermore, it could extend the lifetime of the proteins at the ITIES and facilitate their extraction for further *ex situ* assays.

Here, we have developed a novel method of protein immobilisation within silica matrices generated at electrified liquid-liquid interfaces. Cytochrome *c* (Cyt *c*) a component of the mitochondrial electron transport chain was selected as a model redox protein and encapsulated at the ITIES. The Cyt *c*@silica film was generated at the ITIES following a silica sol-gel process at pH 9.[31,32] The Cyt *c*@silica film formation is based on the electroassisted ion-transfer of cetyltrimethylammonium (CTA^+) that favours the silica precursor condensation at the ITIES.[31] The film condensation occurs at negative potentials avoiding any denaturation induced by hydrophobic interactions with organic anions from the organic phase favoured at positive potentials.[9] We have demonstrated that during the process of silica film formation, a model protein such as Cyt *c* was encapsulated maintaining its conformation. This method may be extended towards the encapsulation of enzymes in a free-standing silica matrix.

Experimental section

Reagents. Cytochrome *c* (Cyt *c*) from bovine heart ≥ 95 % (Cyt c) was purchased from Sigma-Aldrich in the oxidised form (Cyt *c*-Fe(III)) and used without further purification. The organic phase background electrolytes (bis(triphenylphosphoranylidene)ammonium tetrakis(pentafluorophenyl)borate – BATB) and cetyltrimethylammonium tetrakis(pentafluorophenyl)borate (CTA^+TB^-) were precipitated by mixing equimolar amounts of bis(triphenylphosphoranylidene)ammonium chloride (BACl, 97%, Sigma-Aldrich), hexadecyltrimethylammonium bromide (CTAB, 98%, Sigma-Aldrich) and lithium tetrakis(pentafluorophenyl)borate ethyl etherate (LiTB, 98%, Sigma-Aldrich), respectively. Further detail regarded the preparation of the organic electrolytes are given in ref.[32] Trifluorotoluene (TFT, ≥ 99 %, Sigma-Aldrich) and 1,2 dichloroethane (DCE, ≥ 99 %, Alfa Aesar) were used as organic solvents without further purification. Sodium chloride (≥ 98 %, Prolabo) was used as an aqueous electrolyte for the interfacial silica film formation. The silica precursors for the film formation were tetraethoxysilane (TEOS, 98 %, Alfa Aesar) and triethoxymethylsilane (MTES, 99 %, Sigma Aldrich). The pH was adjusted with solutions of 1 M HCl (1 M, volumetric solution, Riedel-de Haen) and 1 M NaOH (from pellets, pure, Riedel-de Haen). Ferric chloride hexahydrate ($FeCl_3 \cdot 6H_2O$, 99–100 %, Fluka) was used to prepare silver/silver chloride *pseudo*-reference electrodes. The electroactivity of encapsulated Cyt *c* was tested at pH 7 using a phosphate buffer solution (PBS) prepared from phosphate buffer saline

tablets purchased from Sigma-Aldrich for a final concentration of 2 mM Phosphate Buffer, 0.54 mM KCl, and 27.4 mM NaCl. Decamethylferrocene (DcMFc, 97%, Sigma Aldrich) was used as purchased as the electron donor to assess the electroactivity of the Cyt *c*@silica films. Purified water (18.2 MΩ cm) was used to prepare all the aqueous solutions, supplied from a Millipore milli-Q water purification system. All other reagents were of the highest grade available and used as received.

Cyt *c*@SiO_2 hydrogel electrogeneration. The sol was prepared as follows: (i) 100 mM of TEOS was hydrolysed in 10 mL of 5 mM NaCl solution at pH 3 under constant stirring for 3 h, after which the hydrolysis was considered complete; (ii) the pH was then increased to pH 9, granting the formation of negatively charged silica oligomers. (iii) 3 mg of bovine heart cyt *c* was dissolved in 4 mL of the hydrolysed solution and used as the aqueous phase in electrochemical cells 1 and 2 (see *cells 1 and 2* in Scheme 1)**.** In the case of Cyt *c*@$MeSiO_2$, part of the TEOS precursor was replaced by methyltriethoxysilane (MTES). The total moles of silica precursor was kept constant (1 mmol). Cyt *c*@SiO_2 and Cyt *c*@$MeSiO_2$ hydrogels were electrogenerated at the liquid-liquid interface in a custom-made four-electrode cell with 3 arms: two Luggin capillaries for the reference electrodes and one arm to add electroactive species into the organic phase (Figure S1). The geometrical area of the interface was 1.53 cm^2.

The interfacial potential difference, $\Delta_o^w \phi$, was controlled with a PINE wavedriver 20 potentiostat (Pine research, USA). Cyt *c*@SiO_2 or Cyt *c*@$MeSiO_2$ hydrogels were electrogenerated by cyclic voltammetry at a slow scan rate (1 or 2 mV s^{-1}). The number of scans varied between 2 and 7. Once formed, the hydrogels were prepared for further characterisation. For *ex situ* Raman and reflective UV-vis spectroscopy, the hydrogel was collected with a spatula and rinsed with a solution of 1:10 ethanol : 1 mM HCl by immersion for 2 hours. This allowed the removal of organic electrolyte and CTA^+ template. Next, the hydrogels were rinsed with a mixture of 1:10 acetone:distilled water and dried overnight in the oven at 40°C. For the *in situ* electrochemical characterisation, the aqueous phase used for the electrogeneration was carefully removed from the electrochemical cell and replaced with 2 mM PBS solution. This process was repeated several times before achieving electrochemical stabilisation of the film in the new aqueous phase electrolyte solution cyclic voltammetry through 20 repetitive scans at 20 mV s^{-1} , see *cell 3* in Scheme 1.

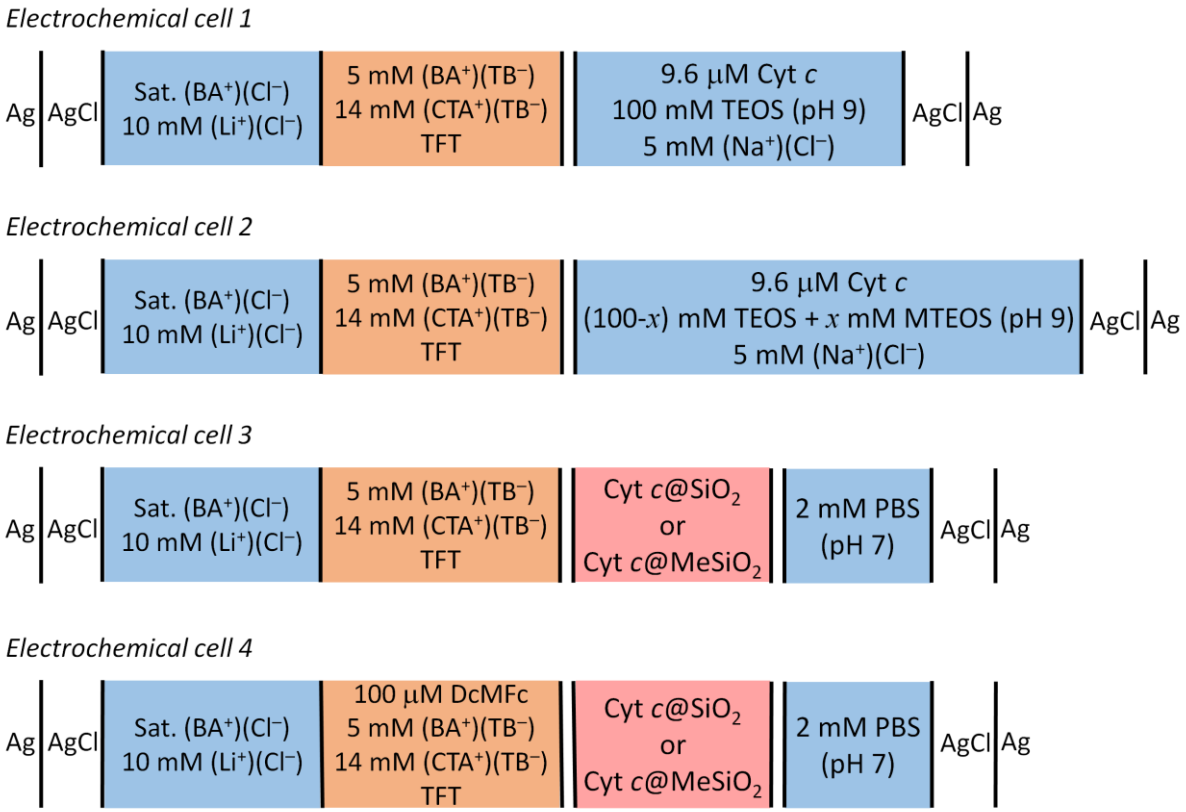

Scheme 1. Four-electrode electrochemical cell configurations investigated.

Cyt *c*@SiO$_2$ and Cyt *c*@MeSiO$_2$ hydrogel characterisation. *In situ* UV-Vis experiments were carried out with a parallel beam configuration using a USB 2000 Fiber Optic Spectrometer (Ocean Optics, USA). The light beam was generated using a DH-2000-BAL deuterium–halogen light source (Ocean Optics, USA), and guided through the optical fiber of 600 nm of diameter (Ocean Optics, USA). The light beam was collimated using optical lenses (Thor-lab, focal length: 2 cm) before and after the transmission of the beam through the electrochemical cell (Figure S2). The potential was controlled using an Autolab PGSTAT204 potentiostat (Metrohm, Switzerland). Confocal Raman spectroscopy measurements were carried out using a WITec 300R spectrometer with a green light laser (532 nm) as excitation source, equipped with a polarising beam splitter for polarised light experiments. The samples were placed on a glass slide and mounted in the focal plane of an Olympus X50 objective. The laser spot was around 2 µm^2. Raman mappings were analysed using WITec project 2.08 software. UV-vis Diffuse Reflectance Spectroscopy (UV-vis DRS) were recorded using a UV-visible-NIR spectrometer (Cary 6000, Agilent), the preparation of the sample (pellets) was 5 mg of sample mixed with 95 mg of KBr. Fluorescence Microscopy was performed using an Olympus BX3-URA fluorescence microscope with a mercury lamp as excitation source and a Power Supply

Unit U-RFL-T. The samples were excited at 360 nm and the fluorescence images were acquired using a 420 nm filter. Interfacial electron transfer reactions at the liquid-liquid interface were investigated after addition of an aliquot of DcMFc to the organic phase. 500 µL of a 1 mM DcMFc solution was added carefully through the third arm of the homemade 4-electrode cell, see *cell 4* in Scheme 1. The organic solution was stirred for 3 min using a PTFE magnetic bar, further details about the electrochemical setup are shown in Figure S1B.

Results and Discussion

Encapsulation of cytochrome *c* within silica matrices by electrochemistry at the ITIES. Cyt *c*@silica films at the ITIES were obtained by cyclic voltammetry. The interfacial transfer of CTA^+ (a cationic surfactant) triggered the condensation of hydrolysed TEOS molecules[31–33] (Figure 1), and Cyt *c* encapsulation. The potential was scanned at 1 mV s^{-1} from the open-circuit potential (ΔE = +0.19 V) towards the negative end of the potential window. The first cycle, showed a sharp negative current appearing between +0.10 and –0.05 V. This current was attributed to the transfer of CTA^+ from the organic to the aqueous phase.[32] Here, the CTA^+ transfer was facilitated by the presence of negatively charged siloxane oligomeric species, which are abundant at pH 9.[34] Once the CTA^+ was transferred to the aqueous phase, these ions led to the formation of charged micelles, which were surrounded by the silica species, facilitating their condensation, and thereby a hydrogel was formed. Upon reversing the scan towards more positive potentials, a peak attributed to a partial back transfer of CTA^+ appeared at +0.28 V.[35] Further changes in polarisation toward more positive potentials have shown a capacitive current attributed to the double layer of the liquid-liquid interface. Repetitive scans have shown a constant increase in the peak intensity attributed to the CTA^+ back-transfer, which indicated the thickening of SiO_2 deposits at the liquid-liquid interface. Control experiments demonstrated that the formation of the silica deposits was not spontaneous; *cell 1* was left for about 1 hour at open circuit potential without the formation of a silica film at the liquid-liquid interface. It is worth mentioning that the electrochemical response of Cyt *c* at pH 9 is featureless within the potential window range used for the Cyt *c*@silica films syntheses (–0.05 to 0.60 V). Therefore, all the voltammetric features shown in Figure1 should be attributed to the silica film formation. As a control, the electrochemical behaviour of Cyt *c* in the absence of CTA^+ and TEOS is shown in Figure S3. Cyt *c* adsorption is observed at the positive end of the potential window around +0.90 V, which is agreement with previous studies.[7–9]

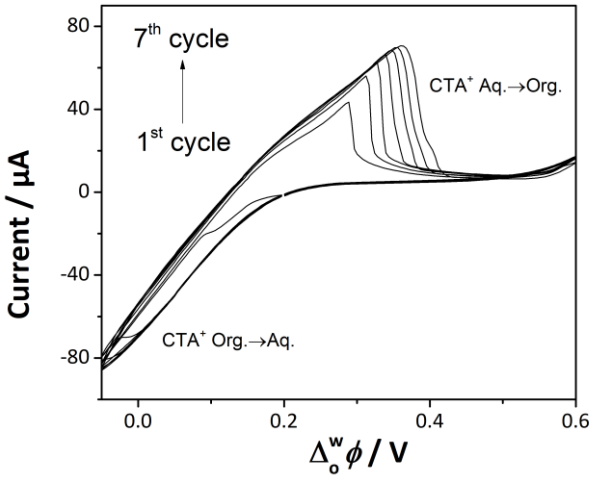

Figure 1. Cyclic voltammogram recorded at the liquid-liquid interface during the Cyt *c*@silica films formation using electrochemical *cell 1* (see Scheme 1) at a scan rate of 1 mV s^{-1}.

Studies on immobilisation of proteins within nanoporous supports have shown that the maximum efficiency of immobilisation was achieved near a protein's isoelectric point (pI). [36,37] Herein, the pH of the aqueous phase was close to the Cyt *c* isoelectric point (pI 9.8) [38,39]. Thus, our conditions of silica film formation should favour the Cyt *c* encapsulation. In order to confirm our hypothesis, the silica sol-gel film formation was followed by *in situ* parallel beam UV-vis absorbance spectroscopy (Figure 2). Here, the beam was parallel to the aqueous side of the liquid-liquid interface where Cyt *c* and the silica precursor were dissolved. Each absorbance spectrum was recorded at –0.04 V. The experimental set-up allowed the recording of UV-vis absorption spectra of Cyt *c* located near the interface during the silica film condensation.

The electronic spectrum of Cyt *c* presents two characteristic bands: (i) the Soret band centred at 407 nm and (ii) the Q band centred at 533 nm. Both bands are attributed to the absorption of the porphyrin chromophore of Cyt *c* (see Figure 2A). The Soret band is attributed to π-π* transitions in the porphyrin ring structure of the Cyt *c*-Fe^{III} (heme centre) and is an indicator of the native-like state of the protein. A blue-shift of the Soret band is commonly attributed to protein denaturation, whereas a red-shift is related to a change in the protein redox state.[40–43] The Q band between 500-565nm showed two absorption bands known as α and β bands, which are poorly defined when the Cyt *c* is in an oxidised state (Fe^{III}).[44,45] The absorbance of the Soret and Q bands increased after each cycle, suggesting that the molar concentration of Cyt *c* near the interface increased after each voltammetric scan. The Soret band was centred at 407 nm and was constant throughout the silica film formation thoroughly

suggesting that Cyt *c* encapsulation occurred without denaturation nor changes in the redox state (Figure 2A).

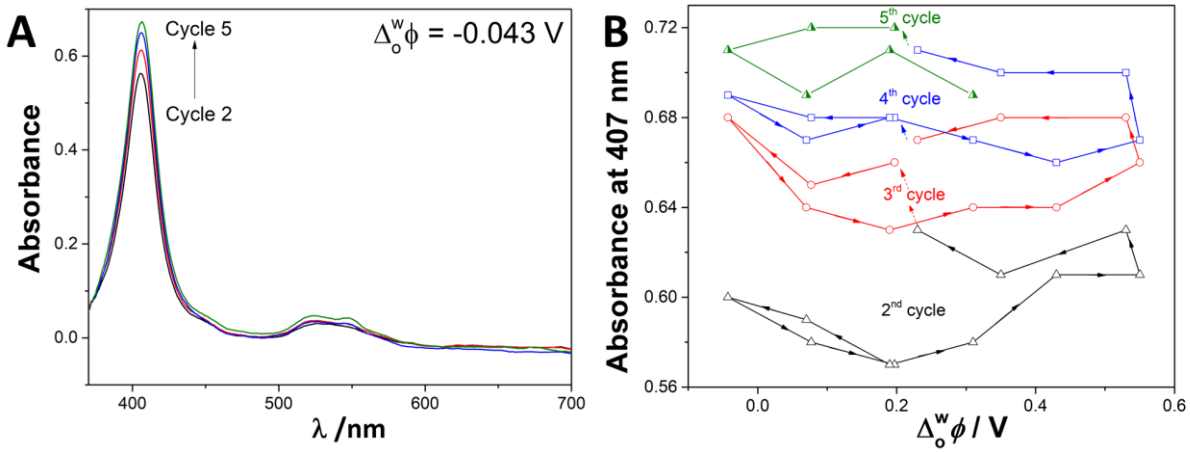

Figure 2. (A) *In situ* UV-vis absorption spectra of Cyt *c* at –0.04 V and **(B)** variation of the absorbance at 407 nm during the cyclic voltammetry cycling experiments performed in Figure 1, using electrochemical *cell 1* (see Scheme 1) at a scan rate of 1 mV s^{-1}.

Figure 2B shows the absorbance of the Soret band *vs.* the potential for each voltammetric cycle. The potential sweep started from +0.20 V towards less positive potentials. The Soret band intensity increased during the second cycle (red line), from +0.20 V towards –0.05 V; confirming that an accumulation of Cyt *c* species occurs in the vicinity of the liquid-liquid interface during negative biasing.[32] When the potential sweep was reversed from –0.05 towards +0.20 V, the intensity of the Soret band decreased, returning to its initial value observed at +0.20 V (Figure 2B). This suggested that partial desorption of Cyt *c* occurred. Another increase of the Soret band absorbance was observed in the potential region from +0.25 to +0.60 V; this was attributed to the presence of positive aqueous species and organic anions (TB^{-}) at the liquid-liquid interface that is favoured at positive potentials (Figure S3). Therefore, a positive biasing favoured the accumulation of Cyt *c* species on the aqueous side of the interface, suggesting a second accumulation step. The reverse scan from +0.60 toward +0.20 V did not show significant changes in the Soret band absorbance, indicating that the concentration of Cyt *c* was constant in the vicinity of the interface. The subsequent cycles presented similar features as the second one. Overall, i*n situ* parallel beam UV-vis experiments suggested that Cyt *c* encapsulation should occur at two different stages of interfacial polarisation: i) at negative potentials while the silica sol-gel formation is formed and ii) at positive potentials due to

electrostatic and hydrophobic interactions with pre-formed silica deposits and TB^- species from the organic phase, respectively.

Spectroscopic characterisation of Cyt *c*@SiO_2 hydrogels. A robust and slightly reddish hydrogel, formed after 7 voltammetric cycles (Figure 3A), was collected from the interface and these Cyt *c*@SiO_2 hydrogel films were characterised by UV-vis DRS and Raman spectroscopy. Further details about sample treatment are described *vide supra* (see sections 2.2 and 2.5). Figure 3B shows the UV-vis spectra of Cyt *c* crystals, Cyt *c*-free silica and Cyt *c*@SiO_2 films. The UV-vis spectrum of Cyt *c* crystals presented a Soret band centred at 407nm and a well defined Q-band (red line). The UV-vis spectrum of encapsulated Cyt c (blue line) presented a Soret band centred at 402 nm, and the absorbance of the Q-band decreased with the appearance of new peaks centred at 509 and 535 nm. The variations of the Q-band absorption and the appearance of new Q band peaks at 509 and 535 nm indicated that the low spin hemes of Cyt *c* were converted to the high spin form.[46,47] This was confirmed by the appearance of a new band centred at 615 nm which was attributed to in-plane charge transfer between the porphyrin and heme iron of high-spin species.[48–50] The change from the low-spin (native Cyt *c*) to the high-spin configuration indicates that the sixth ligand of heme is no longer the Met-80 residue and has been replaced by a different residue or by water molecules. However, encapsulated Cyt *c* still retained its integrity after the immobilisation, which was confirmed by the retention of well-defined Soret band features. Denatured Cyt *c* have would shown a significant decrease in absorbance, a substantial blue shift, and a broadening of the Soret band.[38,49,51] Note that a blue-shift of ca. 5 nm of the Soret band and the decrease of the Q-band intensity could indicate changes in the microenvironment of the encapsulated protein caused by the loss of the water after the drying process.[52,53] Indeed, a decay of the Q-band might be related to strong electrostatic interactions within the silica pores.[54] The UV-vis diffuse reflectance spectrum of pure silica deposits (Figure 3B, black curve) did not show any features at 407 nm or in the 500 – 600 nm region. Therefore, the spectrum taken for the encapsulated Cyt *c* must be purely attributed to electronic transitions of the heme group.

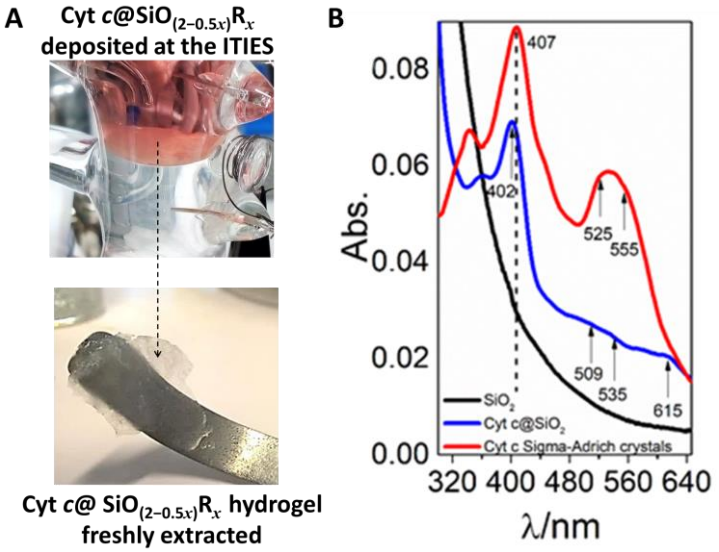

Figure 3. (A) Top: Photograph of the Cyt *c*@ SiO_2 films deposited at the interface after 7 repetitive scans at 1 mV s^{-1} , bottom: Cyt *c*@ SiO_2 film collected at the liquid-liquid interface. (B) UV-vis DRS of pure Cyt *c* powder (red curve), Cyt *c*@ SiO_2 films after CTA^+ extraction (blue curve) and SiO_2 deposits in the absence of Cyt *c* (black curve).

UV-vis DRS studies have shown that Cyt *c* species were successfully immobilised within the silica films; however, the distribution of the protein within the silica matrix was still uncertain. Therefore, Raman scattering measurements were performed to study the distribution and the structural changes of Cyt c within the silica films.[55–58] Most of the Raman vibrational modes of Cyt *c* have been described in detail by Spiro *et al.* [55,56,59] and assigned to active vibrational modes of the heme group ($\pi \rightarrow \pi^*$ transition in the porphyrin ring). Figure 4A shows the Raman spectra of Cyt *c* crystals (red line), Cyt *c*@SiO_2 (blue line) and SiO_2 (black line) films. The vibrational studies were performed in the range of 1000 and 1650 cm^{-1} since most of the relevant Raman modes belong to this vibrational window.

The Raman spectrum of Cyt *c* crystals (red line) showed a vibrational mode at 1374 cm^{-1} (ν , pyrrole half-$ring_{sys}$), known as the ν_4 vibrational mode and assigned to the porphyrin ring breathing mode.[60] This band was considered an indicator of the oxidation state of the heme since it followed the electron density of the iron porphyrin. The vibrational modes at 1585 and 1639 cm^{-1} known as ν_2 and ν_{10} , respectively, corresponded to Raman modes of the amide-I symmetric stretching (C_β-C_β) and (C_α-C_m).[58] Here, the band ν_2 is considered as a spin-state marker, whereas ν_{10} is considered a band sensitive to structural changes in the protein.[61] Thus, the Cyt *c* crystals were oxidised and in their native state (Cyt *c* Fe^{III}). It is worth mentioning

that any down-shift of the ν_4 and ν_{10} bands could be attributed to changes in the oxidation state or in the structural conformation of Cyt *c*, respectively.

The Raman spectrum of a Cyt *c*@SiO_2 film (blue line) revealed well-defined ν_4 and ν_{10} modes. These bands did not overlap with the SiO_2 stretching bands (see black line). The appearance of a broad band centred ca. 1596 cm^{-1} indicated the presence of mixed tertiary structure and intermingled α-helical and β-sheet secondary structures.[58] These conformational changes were attributed to the strong interactions between the silica walls and the Cyt *c*. With regards to the ν_4 mode centred at 1374 cm^{-1}, this band did not show any shift for the Cyt *c*@SiO_2 film indicating that the encapsulated protein kept its initial oxidation state. The Raman spectrum for the Cyt *c*-free silica film (black line) has shown bands centred at 1091 and 1452 cm^{-1}, these bands were attributed to C-O asymmetric stretching and CH_3 asymmetric deformation of partially hydrolysed TEOS, respectively.[62]

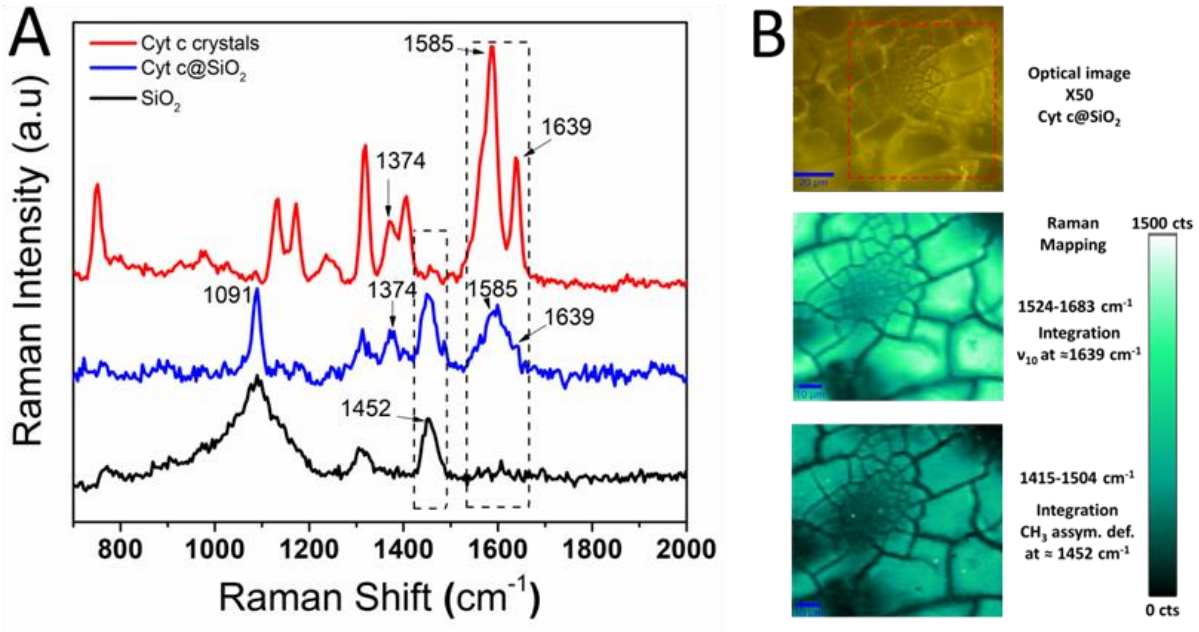

Figure 4. (A) Raman spectra of Cyt *c* crystals (red curve), Cyt *c*@ SiO_2 (blue curve) and SiO_2 deposit (black curve). (B) Optical image of Cyt *c*@ SiO_2 (top), Raman mapping considering a band specific to Cyt *c* (ν_{10} at 1639 cm^{-1}, middle) and a band specific to SiO_2 (CH_3 asymmetric deformation of partially hydrolysed TEOS at 1452 cm^{-1}, bottom) as the integration peaks, respectively.

The primary concern during the encapsulation process was Cyt *c* agglomeration within the silica matrix. Therefore, Raman mapping was used to verify the even distribution of Cyt *c* at the microscopic level. To do so, we have selected one Raman band specific to Cyt *c* and

another one for SiO_2. We used the broad band centred at 1596 cm^{-1}, which included the pair of peaks centred at 1585 and 1639 cm^{-1} attributed to the vibration modes ν_2 and ν_{10} of Cyt *c*. We carried out the integration of the band centred at 1452 cm^{-1} to identify the SiO_2-rich region of the sample. The mapping of Cyt *c*@SiO_2 pointed out that both SiO_2 and Cyt *c* were evenly distributed within the sample, suggesting a homogeneous distribution of Cyt *c* within the silica during the silica deposition process.

Experiments of fluorescence microscopy confirmed the results obtained by Raman spectroscopy suggesting the presence of a mixed tertiary structure of Cyt *c* species within the silica film (Figure 5). Tryptophan fluorescence is a convenient method to investigate the local conformation of a protein.[63,64] Tryptophan-59 of Cyt *c* forms a hydrogen-bond to one of the propionic groups of the heme centre. In the native state, the fluorescence emission intensity of this group is low due to quenching of the emission signal.[65–67] However, a partial unfolding of the protein decreases the fluorescence quenching, and the emission intensity of Tryptophan-59 became measurable.[65] The fluorescent emission micrograph did not show fluorescent regions, suggesting that Cyt *c* was encapsulated in a native-like state, as suggested by UV-vis DRS and Raman studies. The Cyt *c*@SiO_2 film was then treated using a mixture 1:1 of 0.1 M HCl:ethanol for two hours under constant stirring to chemically induce denaturing of the encapsulated protein. After application of this chemical treatment, the appearance of the film was not affected. However, the emission intensity increased noticeably all over the film (Figure 5B), with several fluorescent hot spots attributed to the unfolded structure of Cyt *c* observed.

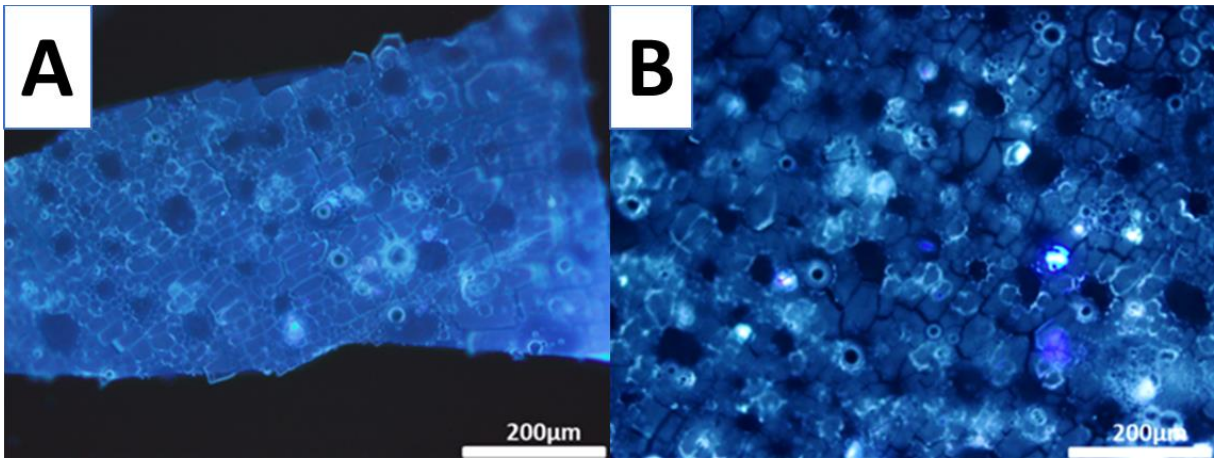

Figure 5. Fluorescence micrographs of Cyt *c*@SiO_2 deposits before **(A)** and after **(B)** 0.1 M HCl:ethanol treatment.

Based on the *ex situ* spectroscopic characterisation of the Cyt *c*@SiO_2 hydrogel, Cyt *c* retained its tertiary structure and did not unfold during the encapsulation process at the ITIES. This result suggests that other proteins (enzymes, monoclonal antibodies, among others) could be immobilised and studied at the interface following a similar *in situ* sol-gel encapsulation process at the ITIES.

Electrochemical characterisation of Cyt *c*@SiO_2 hydrogels. In our recent breakthrough study we have shown that,in the absence of silica, Cyt *c* adsorbs on the interface by the application of an interfacial potential difference higher than the PZC.[23] Under positive polarization of the interface, Cyt *c* is oriented with the active heme group facing towards the organic phase, where it is accessible for an electron transfer reaction with the organic reductant decamethylferrocene (DcMFc). Cyclic voltammetry in the presence of Cyt *c* and DcMFc showed two processes: (i) a rise of current at an onset potential at +0.50 V and (ii) a reversible ion transfer at a half-wave potential at +0.20 V (Figure S4). The first process was attributed to the interfacial electron transfer reaction between Cyt *c* and DcMFc, while the second process was linked to the transfer of the $DcMFc^+$ cations generated. The interfacial electron transfer is the consequence of O_2 catalytic reduction by Cyt *c* partially denatured by interfacial adsorption and its interaction with organic TB^-. In its native state, Cyt *c* does not catalyse O_2 reduction, but upon partial denaturation by polarisation of the ITIES, Cyt c becomes a potential O_2 reduction catalyst.[23]

Ex situ spectroscopic characterisation, reported in section 3.2, suggested that Cyt *c* encapsulated in silica (Cyt *c*@SiO_2) retained its native conformation and hence should not catalyse O_2 reduction. A Cyt *c*@SiO_2 hydrogel was thus prepared by cyclic voltammetry using electrochemical *cell 2*. Once the Cyt *c*@SiO_2 was formed, the aqueous phase was carefully replaced with a phosphate buffer solution at pH 7 (Figure S5). The silica film remained intact after the replacement of the aqueous solution. Indeed, it did not show macroscopic defects; it was flexible and robust, with waves or curls at the interface suggesting a membrane-like behaviour. A stable cyclic voltammetry signal was obtained after 20 repetitive cycles. The stabilised CV presented a featureless blank CV with a typical ion transfer of background electrolyte at both negative and positive end potentials (Figure S5). After the addition of 100 µM of DcMFc to the organic phase, no electrocatalytic activity towards O_2 reduction was observed, confirming that Cyt *c* kept its native conformation during the encapsulation (Figure 6). This may be ascribed to electrostatic interactions between Cyt *c* and the surface of the silica pores,[28] avoiding further hydrophobic interactions and partial protein denaturation.

Since the environment nearby a protein plays a major role in its electroactivity,[27,28,68] Cyt *c* species were encapsulated within organic-inorganic hybrid silica films. A hybrid Cyt *c*@Silica film was prepared from a sol which contained 10 % of methyltriethoxysilane (MTEOS). These Cyt *c*@$MeSiO_2$ films presented an interfacial electroactivity in the presence of DcMFc with an onset of current at +0.45 V, attributed to O_2 reduction (Figure 6). The interfacial electroactivity observed with hybrid Cyt *c*@$MeSiO_2$ films might be due to the higher hydrophobicity, allowing organic phase to diffuse through the hybrid silica gel and thus causing partial denaturation of the encapsulated Cyt *c*. These experiments show that control of Cyt *c*'s immediate environment can protect the biomolecule from denaturation despite the application of a positive interfacial potential difference and the close proximity of the organic phase.

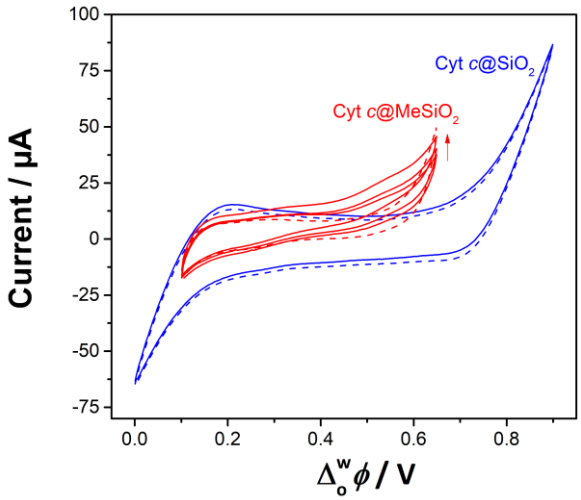

Figure 6. Cyclic voltammograms of Cyt *c*@SiO_2 (blue curve) and Cyt *c*@$MeSiO_2$ (red curves) modified ITIES in the absence (dashed curves) and in the presence (solid curves) of 100 µM DcMFc in the organic phase. They cyclic voltammetry was performed using electrochemical *cell 4* (see Scheme 1) at a scan rate of 20 mV s^{-1}. The arrow represent the current evolution with the repetition of scans in the case of Cyt *c*@$MeSiO_2$.

Conclusions

Cyt *c* was encapsulated in a silica hydrogel during the cycling of the potential window, which allowed subsequent silica condensation and Cyt *c* adsorption. This two-step electrochemical process was followed by *in situ* UV-vis absorption spectroscopy. After the hydrogel formation, *ex situ* spectroscopic characterisation (confocal Raman microscopy, fluorescence spectroscopy and UV-vis diffusive reflectance spectroscopy) showed that Cyt *c* was deposited in its native state. This was also confirmed by the absence of O_2 catalysed by

denatured Cyt *c* at the ITIES. This method for the encapsulation of Cyt *c* at soft polarised interfaces could be used for other types of proteins in the field of bioelectrosynthesis or bioelectrocatalysis, where the low water solubility of hydrophobic substrates or products may limit the conversion rate of chiral compounds of pharmaceutical interest.

Acknowledgements

The authors are grateful for travel support of the Irish Research Council and Campus France between the French and Irish groups through their joint ULYSSES programme. GH, MD and AW are grateful to the French Programme Investissement d'Avenir (PIA) "Lorraine Université d'Excellence" (Reference N° ANR-15-IDEX-04-LUE) and to the Agence Nationale de la Recherche (Hyperion project, grant number: ANR-14-CE14-0002-01) for partial funding of the research. MDS acknowledges Science Foundation Ireland (SFI) under Grant no. 13/SIRG/2137 and the European Research Council (ERC) through a Starting Grant (Agreement no. 716792). AGQ acknowledges funding received from an Irish Research Council (IRC) Government of Ireland Postdoctoral Fellowship Award (Grant Number GOIPD/2018/252).

References

(1) Gray, C. J.; Weissenborn, M. J.; Eyers, C. E.; Flitsch, S. L. Enzymatic Reactions on Immobilised Substrates. *Chem. Soc. Rev.* **2013**, *42*, 6378–6405. https://doi.org/10.1039/c3cs60018a.

(2) Sheldon, R. A.; van Pelt, S. Enzyme Immobilisation in Biocatalysis: Why, What and How. *Chem. Soc. Rev.* **2013**, *42*, 6223–6235. https://doi.org/10.1039/c3cs60075k.

(3) Pinholt, C.; Hartvig, R. A.; Medlicott, N. J.; Jorgensen, L. The Importance of Interfaces in Protein Drug Delivery - Why Is Protein Adsorption of Interest in Pharmaceutical Formulations? *Expert Opin. Drug Deliv.* **2011**, *8*, 949–964. https://doi.org/10.1517/17425247.2011.577062.

(4) Chen, H.; Simoska, O.; Lim, K.; Grattieri, M.; Yuan, M.; Dong, F.; Lee, Y. S.; Beaver, K.; Weliwatte, S.; Gaffney, E. M.; Minteer, S. D. Fundamentals, Applications, and Future Directions of Bioelectrocatalysis. *Chem. Rev.* **2020**. https://doi.org/10.1021/acs.chemrev.0c00472.

(5) Arrigan, D. W. M. Voltammetry of Proteins at Liquid-Liquid Interfaces. *Annu. Reports Prog. Chem. - Sect. C* **2013**, *109*, 167–188. https://doi.org/10.1039/c3pc90007j.

(6) Arrigan, D. W. M.; Hackett, M. J.; Mancera, R. L. Electrochemistry of Proteins at the

Interface between Two Immiscible Electrolyte Solutions. *Curr. Opin. Electrochem.* **2018**, *12*, 27–32. https://doi.org/10.1016/j.coelec.2018.07.012.

(7) Shinshi, M.; Sugihara, T.; Osakai, T.; Goto, M. Electrochemical Extraction of Proteins by Reverse Micelle Formation. *Langmuir* **2006**, *22*, 5937–5944. https://doi.org/10.1021/la060858n.

(8) Shinshi, M.; Sugihara, T.; Osakai, T.; Goto, M. Erratum: Electrochemical Extraction of Proteins by Reverse Micelle Formation (Langmuir (2006) 22 (5937-5944)). *Langmuir* **2006**, *22*, 8614. https://doi.org/10.1021/la062188r.

(9) Alvarez de Eulate, E.; O'Sullivan, S.; Arrigan, D. W. M. Electrochemically Induced Formation of Cytochrome c Oligomers at Soft Interfaces. *ChemElectroChem* **2017**, *4*, 898–904. https://doi.org/10.1002/celc.201600851.

(10) Kivlehan, F.; Lanyon, Y. H.; Arrigan, D. W. M. Electrochemical Study of Insulin at the Polarized Liquid-Liquid Interface. *Langmuir* **2008**, *24*, 9876–9882. https://doi.org/10.1021/la800842f.

(11) Herzog, G.; Kam, V.; Arrigan, D. W. M. Electrochemical Behaviour of Haemoglobin at the Liquid/Liquid Interface. *Electrochim. Acta* **2008**, *53*, 7204–7209. https://doi.org/10.1016/j.electacta.2008.04.072.

(12) Herzog, G.; Moujahid, W.; Strutwolf, J.; Arrigan, D. W. M. Interactions of Proteins with Small Ionised Molecules: Electrochemical Adsorption and Facilitated Ion Transfer Voltammetry of Haemoglobin at the Liquidliquid Interface. *Analyst* **2009**, *134*, 1608–1613. https://doi.org/10.1039/b905441n.

(13) Scanlon, M. D.; Jennings, E.; Arrigan, D. W. M. Electrochemical Behaviour of Hen-Egg-White Lysozyme at the Polarised Water/1, 2-Dichloroethane Interface. *Phys. Chem. Chem. Phys.* **2009**, *11*, 2272–2280. https://doi.org/10.1039/b815589e.

(14) O'Sullivan, S.; Arrigan, D. W. M. Electrochemical Behaviour of Myoglobin at an Array of Microscopic Liquid-Liquid Interfaces. *Electrochim. Acta* **2012**, *77*, 71–76. https://doi.org/10.1016/j.electacta.2012.05.070.

(15) Matsui, R.; Sakaki, T.; Osakai, T. Label-Free Amperometric Detection of Albumin with an Oil/Water-Type Flow Cell for Urine Protein Analysis. *Electroanalysis* **2012**, *24*, 1164–1169. https://doi.org/10.1002/elan.201200048.

(16) Sakae, H.; Toda, Y.; Yokoyama, T. Electrochemical Behavior of Ferritin at the Polarized Water|1,2-Dichloroethane Interface. *Electrochem. Commun.* **2018**, *90*, 83–86. https://doi.org/10.1016/j.elecom.2018.04.010.

(17) Felisilda, B. M. B.; Arrigan, D. W. M. Electroactivity of Aptamer at Soft

Microinterface Arrays. *Anal. Chem.* **2018**, *90*, 8470–8477. https://doi.org/10.1021/acs.analchem.8b01172.

(18) Hartvig, R. A.; Méndez, M. A.; Weert, M. Van De; Jorgensen, L.; Østergaard, J.; Girault, H. H.; Jensen, H. Interfacial Complexes between a Protein and Lipophilic Ions at an Oil-Water Interface. *Anal. Chem.* **2010**, *82*, 7699–7705. https://doi.org/10.1021/ac101528r.

(19) Alvarez de Eulate, E.; Qiao, L.; Scanlon, M. D.; Girault, H. H.; Arrigan, D. W. M. Fingerprinting the Tertiary Structure of Electroadsorbed Lysozyme at Soft Interfaces by Electrostatic Spray Ionization Mass Spectrometry. *Chem. Commun.* **2014**, *50*, 11829–11832. https://doi.org/10.1039/c4cc05545d.

(20) Booth, S. G.; Felisilda, B. M. B.; Alvarez De Eulate, E.; Gustafsson, O. J. R.; Arooj, M.; Mancera, R. L.; Dryfe, R. A. W.; Hackett, M. J.; Booth, S. G. Secondary Structural Changes in Proteins as a Result of Electroadsorption at Aqueous-Organogel Interfaces. *Langmuir* **2019**, *35*, 5821–5829. https://doi.org/10.1021/acs.langmuir.8b04227.

(21) Arooj, M.; Gandhi, N. S.; Kreck, C. A.; Arrigan, D. W. M.; Mancera, R. L. Adsorption and Unfolding of Lysozyme at a Polarized Aqueous-Organic Liquid Interface. *J. Phys. Chem. B* **2016**, *120*, 3100–3112. https://doi.org/10.1021/acs.jpcb.6b00536.

(22) Arooj, M.; Arrigan, D. W. M.; Mancera, R. L. Characterization of Protein-Facilitated Ion-Transfer Mechanism at a Polarized Aqueous/Organic Interface. *J. Phys. Chem. B* **2019**, *123*, 7436–7444. https://doi.org/10.1021/acs.jpcb.9b04746.

(23) Gamero-Quijano, A.; Bhattacharya, S.; Cazade, P. A.; Molina-Osorio, A. F.; Beecher, C.; Djeghader, A.; Soulimane, T.; Dossot, M.; Thompson, D.; Herzog, G.; Scanlon, M. D. Modulating the Pro-Apoptotic Activity of Cytochrome c at a Biomimetic Electrified Interface. *Submitted* **2021**.

(24) Burgos, M. I.; Ochoa, A.; Perillo, M. A. β-Sheet to α-Helix Conversion and Thermal Stability of β-Galactosidase Encapsulated in a Nanoporous Silica Gel. *Biochem. Biophys. Res. Commun.* **2019**, *508*, 270–274. https://doi.org/10.1016/j.bbrc.2018.11.077.

(25) Nguyen, L.; Döblinger, M.; Liedl, T.; Heuer-Jungemann, A. DNA-Origami-Templated Silica Growth by Sol–Gel Chemistry. *Angew. Chemie - Int. Ed.* **2019**, *58*, 912–916. https://doi.org/10.1002/anie.201811323.

(26) Catauro, M.; Ciprioti, S. V. *Sol-Gel Synthesis and Characterizationof Hybrid Materials for Biomedical Applications*; Springer Singapore, 2019. https://doi.org/10.1007/978-981-13-0989-2.

(27) López-Bernabeu, S.; Gamero-Quijano, A.; Huerta, F.; Morallón, E.; Montilla, F. Enhancement of the Direct Electron Transfer to Encapsulated Cytochrome c by Electrochemical Functionalization with a Conducting Polymer. *J. Electroanal. Chem.* **2017**, *793*, 34–40. https://doi.org/10.1016/j.jelechem.2016.12.044.

(28) Gamero-Quijano, A.; Huerta, F.; Morallón, E.; Montilla, F. Modulation of the Silica Sol-Gel Composition for the Promotion of Direct Electron Transfer to Encapsulated Cytochrome C. *Langmuir* **2014**, *30*, 10531–10538. https://doi.org/10.1021/la5023517.

(29) Poltorak, L.; van der Meijden, N.; Oonk, S.; Sudhölter, E. J. R.; de Puit, M. Acid Phosphatase Behaviour at an Electrified Soft Junction and Its Interfacial Co-Deposition with Silica. *Electrochem. Commun.* **2018**, *94*, 27–30. https://doi.org/10.1016/j.elecom.2018.07.022.

(30) Poltorak, L.; van der Meijden, N.; Skrzypek, S.; Sudhölter, E. J. R.; de Puit, M. Co-Deposition of Silica and Proteins at the Interface between Two Immiscible Electrolyte Solutions. *Bioelectrochemistry* **2020**, *134*, 107529. https://doi.org/10.1016/j.bioelechem.2020.107529.

(31) Poltorak, L.; Herzog, G.; Walcarius, A. In-Situ Formation of Mesoporous Silica Films Controlled by Ion Transfer Voltammetry at the Polarized Liquid-Liquid Interface. *Electrochem. Commun.* **2013**, *37*, 76–79. https://doi.org/10.1016/j.elecom.2013.10.018.

(32) Poltorak, L.; Herzog, G.; Walcarius, A. Electrochemically Assisted Generation of Silica Deposits Using a Surfactant Template at Liquid/Liquid Microinterfaces. *Langmuir* **2014**, *30*, 11453–11463. https://doi.org/10.1021/la501938g.

(33) Mareček, V.; Jänchenová, H. Electrochemically Controlled Formation of a Silicate Membrane at a Liquid|liquid Interface. *J. Electroanal. Chem.* **2003**, *558*, 119–123. https://doi.org/10.1016/S0022-0728(03)00386-3.

(34) Kickelbick, G. *Hybrid Materials, Synthesis, Characterization and Applications*; Kickelbick, G., Ed.; WILEY-VCH Verlag GmbH: Germany, 2007.

(35) Poltorak, L.; Dossot, M.; Herzog, G.; Walcarius, A. Interfacial Processes Studied by Coupling Electrochemistry at the Polarised Liquid-Liquid Interface with in Situ Confocal Raman Spectroscopy. *Phys. Chem. Chem. Phys.* **2014**, *16*, 26955–26962. https://doi.org/10.1039/c4cp03254c.

(36) Sang, L.-C.; Vinu, A.; Coppens, M.-O. General Description of the Adsorption of Proteins at Their Iso-Electric Point in Nanoporous Materials. *Langmuir* **2011**, *27*, 13828–13837. https://doi.org/10.1021/la202907f.

(37) Moerz, S. T.; Huber, P. Protein Adsorption into Mesopores: A Combination of

Electrostatic Interaction, Counterion Release, and van Der Waals Forces. *Langmuir* **2014**, *30*, 2729–2737. https://doi.org/10.1021/la404947j.

(38) Vinu, A.; Murugesan, V.; Tangermann, O.; Hartmann, M. Adsorption of Cytochrome c on Mesoporous Molecular Sieves: Influence of PH, Pore Diameter, and Aluminum Incorporation. *Chem. Mater.* **2004**, *16*, 3056–3065. https://doi.org/10.1021/cm049718u.

(39) Hristova, S.; Zhivkov, A.; Atanasov, B. Electrostatics of Horse Heart Cytochrome c and Montmorillonite Monolamellar Plate. *Biotechnol. Biotechnol. Equip.* **2009**, *23*, 568–571. https://doi.org/10.1080/13102818.2009.10818489.

(40) Hirota, S.; Hattori, Y.; Nagao, S.; Taketa, M.; Komori, H.; Kamikubo, H.; Wang, Z.; Takahashi, I.; Negi, S.; Sugiura, Y.; Kataoka, M.; Higuchi, Y. Cytochrome c Polymerization by Successive Domain Swapping at the C-Terminal Helix. *Proc. Natl. Acad. Sci.* **2010**, *107*, 12854–12859. https://doi.org/10.1073/pnas.1001839107.

(41) Wang, Z.; Ando, Y.; Nugraheni, A. D.; Ren, C.; Nagao, S.; Hirota, S. Self-Oxidation of Cytochrome c at Methionine80 with Molecular Oxygen Induced by Cleavage of the Met-Heme Iron Bond. *Mol. Biosyst.* **2014**, *10*, 3130–3137. https://doi.org/10.1039/c4mb00285g.

(42) Gamero-Quijano, A.; Huerta, F.; Morallo, E.; Montilla, F.; Morallón, E.; Montilla, F. Modulation of the Silica Sol − Gel Composition for the Promotion of Direct Electron Transfer to Encapsulated Cytochrome C. *Langmuir* **2014**, *30*, 10531–10538. https://doi.org/10.1021/la5023517.

(43) Zhao, H.-Z.; Du, Q.; Li, Z.-S.; Yang, Q.-Z. Mechanisms for the Direct Electron Transfer of Cytochrome c Induced by Multi-Walled Carbon Nanotubes. *Sensors (Basel).* **2012**, *12*, 10450–10462. https://doi.org/10.3390/s120810450.

(44) Suemoto, T.; Ebihara, H.; Nakao, H.; Nakajima, M. Observation of Ultrafast Q-Band Fluorescence in Horse Heart Cytochrome c in Reduced and Oxidized Forms. *J. Chem. Phys.* **2011**, *134*. https://doi.org/10.1063/1.3518370.

(45) Collinson, M.; Bowden, E. F. UV-Visible Spectroscopy of Adsorbed Cytochrome c on Tin Oxide Electrodes. *Anal. Chem.* **1992**, *64*, 1470–1476. https://doi.org/10.1021/ac00037a028.

(46) Liu, H.; Tian, Y.; Deng, Z. Morphology-Dependent Electrochemistry and Electrocatalytical Activity of Cytochrome C. *Langmuir* **2007**, *23*, 9487–9494. https://doi.org/10.1021/la700817y.

(47) Cheng, S. H.; Kao, K. C.; Liao, W. N.; Chen, L. M.; Mou, C. Y.; Lee, C. H. Site-

Specific Immobilization of Cytochrome c on Mesoporous Silica through Metal Affinity Adsorption to Enhance Activity and Stability. *New J. Chem.* **2011**, *35*, 1809–1816. https://doi.org/10.1039/c1nj20255c.

(48) Lee, C. H.; Mou, C. Y.; Ke, S. C.; Lin, T. S. Effect of Spin Configuration on the Reactivity of Cytochrome c Immobilized in Mesoporous Silica. *Mol. Phys.* **2006**, *104*, 1635–1641. https://doi.org/10.1080/00268970500501045.

(49) Lee, C. H.; Lang, J.; Yen, C. W.; Shih, P. C.; Lin, T. S.; Mou, C. Y. Enhancing Stability and Oxidation Activity of Cytochrome c by Immobilization in the Nanochannels of Mesoporous Aluminosilicates. *J. Phys. Chem. B* **2005**, *109*, 12277–12286. https://doi.org/10.1021/jp050535k.

(50) Kao, K. C.; Lee, C. H.; Lin, T. S.; Mou, C. Y. Cytochrome c Covalently Immobilized on Mesoporous Silicas as a Peroxidase: Orientation Effect. *J. Mater. Chem.* **2010**, *20*, 4653–4662. https://doi.org/10.1039/b925331a.

(51) Fedurco, M.; Augustynski, J.; Indiani, C.; Smulevich, G.; Antalík, M.; Bánó, M.; Sedlák, E.; Glascock, M. C.; Dawson, J. H. The Heme Iron Coordination of Unfolded Ferric and Ferrous Cytochrome c in Neutral and Acidic Urea Solutions. Spectroscopic and Electrochemical Studies. *Biochim. Biophys. Acta - Proteins Proteomics* **2004**, *1703*, 31–41. https://doi.org/10.1016/j.bbapap.2004.09.013.

(52) Dave, B. C.; Miller, J. M.; Dunn, B.; Valentine, J. S.; Zink, J. I. Encapsulation of Proteins in Bulk and Thin Film Sol-Gel Matrices. *J. Sol-Gel Sci. Technol.* **1997**, *8*, 629–634. https://doi.org/10.1007/BF02436913.

(53) Lan, E. H.; Dave, B. C.; Fukuto, J. M.; Dunn, B.; Zink, J. I.; Valentine, J. S. Synthesis of Sol-Gel Encapsulated Heme Proteins with Chemical Sensing Properties. *J. Mater. Chem.* **1999**, *9*, 45–53. https://doi.org/10.1039/a805541f.

(54) Droghetti, E.; Oellerich, S.; Hildebrandt, P.; Smulevich, G. Heme Coordination States of Unfolded Ferrous Cytochrome C. *Biophys. J.* **2006**, *91*, 3022–3031. https://doi.org/10.1529/biophysj.105.079749.

(55) Spiro, T. G.; Strekas, T. C. Resonance Raman Spectra of Heme Proteins. Effects of Oxidation and Spin State. *J. Am. Chem. Soc.* **1974**, *96*, 338–345. https://doi.org/10.1021/ja00809a004.

(56) Strekas, T. C.; Spiro, T. G. Cytochrome c: Resonance Raman Spectra. *BBA - Protein Struct.* **1972**, *278*, 188–192. https://doi.org/10.1016/0005-2795(72)90121-3.

(57) Döpner, S.; Hildebrandt, P.; Resell, F. I.; Mauk, A. G. Alkaline Conformational Transitions of Ferricytochrome c Studied by Resonance Raman Spectroscopy. *J. Am.*

Chem. Soc. **1998**, *120*, 11246–11255. https://doi.org/10.1021/ja9717572.

(58) Kitt, J. P.; Bryce, D. A.; Minteer, S. D.; Harris, J. M. Raman Spectroscopy Reveals Selective Interactions of Cytochrome c with Cardiolipin That Correlate with Membrane Permeability. *J. Am. Chem. Soc.* **2017**, *139*, 3851–3860. https://doi.org/10.1021/jacs.7b00238.

(59) Hu, S.; Spiro, T. G.; Morris, I. K.; Singh, J. P.; Smith, K. M. Complete Assignment of Cytochrome c Resonance Raman Spectra via Enzymatic Reconstitution with Isotopically Labeled Hemes. *J. Am. Chem. Soc.* **1993**, *115*, 12446–12458. https://doi.org/10.1021/ja00079a028.

(60) Jordan, T.; Eads, J. C.; Spiro, T. G. Secondary and Tertiary Structure of the A-State of Cytochrome c from Resonance Raman Spectroscopy. *Protein Sci.* **1995**, *4*, 716–728. https://doi.org/10.1002/pro.5560040411.

(61) Choi, Jungkweon; Cho, Dae Won; Tojo, S. et al.; Choi, J.; Cho, D. W.; Tojo, S.; Fujitsuka, M.; Majima, T. Configurational Changes of Heme Followed of Cytochrome c Folding Reaction. *Mol. BioSyst.* **1998**, *11*, 182. https://doi.org/10.1080/10420159808220285.

(62) Matos, M. C.; Ilharco, L. M.; Almeida, R. M. The Evolution of TEOS to Silica Gel and Glass by Vibrational Spectroscopy. *J. Non. Cryst. Solids* **1992**, *147–148*, 232–237. https://doi.org/10.1016/S0022-3093(05)80622-2.

(63) Moore, G. R.; Pettigrew, G. W. *Cytochromes c, Evolutionary, Structural and Physicochemical Aspects*, 1st editio.; Springer-Verlag, 1990.

(64) Hlady, V.; Buijs, J.; Jennissen, H. *Methods for Studying Protein Adsorption*; 1999; Vol. 309.

(65) Haldar, S.; Sil, P.; Thangamuniyandi, M.; Chattopadhyay, K. Conversion of Amyloid Fibrils of Cytochrome c to Mature Nanorods through a Honeycomb Morphology. *Langmuir* **2015**, *31*, 4213–4223. https://doi.org/10.1021/la5029993.

(66) Fisher, W. R.; Taniuchi, Hiroshi; Anfinsen, B. On the Role of Heme in the Formation of the Strucure of Cytochrome C. *J. Biol. Chem.* **1973**, *248*, 3188–3195.

(67) Weber, G.; Teale, F. J. W. Electronic Energy Transfer in Haem Proteins. *Discuss. Faraday Soc.* **1959**, *27*, 134–141. https://doi.org/10.1039/qr9662000403.

(68) López-Bernabeu, S.; Huerta, F.; Morallón, E.; Montilla, F. Direct Electron Transfer to Cytochrome *c* Induced by a Conducting Polymer. *J. Phys. Chem. C* **2017**, *121*, 15870–15879. https://doi.org/10.1021/acs.jpcc.7b05204.